



Influence of the nature of organic components in dinuclear copper(II) pivalates on the composition of thermal decomposition products

Irina Fomina^{a,*}, Zhanna Dobrokhotova^a, Grygory Aleksandrov^a, Artem Bogomyakov^{b,1}, Matvey Fedin^{b,1}, Alexander Dolganov^{c,2}, Tatyana Magdesieva^{c,2}, Vladimir Novotortsev^a, Igor Eremenko^a

^aN.S. Kurnakov Institute of General and Inorganic Chemistry, Russian Academy of Sciences, Leninsky prosp. 31, 119991 Moscow, GSP-1, Russian Federation

^bInternational Tomography Center, Siberian Branch, Russian Academy of Sciences, Institutskaya str. 3a, 630090 Novosibirsk, Russian Federation

^cDepartment of Chemistry, M. V. Lomonosov Moscow State University, Leninskie Gory 1/3, 119991 Moscow, GSP-1, Russian Federation

ARTICLE INFO

Article history:

Received 8 October 2009

Accepted 11 February 2010

Available online 17 February 2010

Keywords:

Copper pivalates

Aminopyridine ligands

Synthesis

X-ray diffraction study

Magnetic properties

Electrochemical behavior

Solid-state thermal decomposition

ABSTRACT

Tetrabridged dinuclear complexes $((2\text{-NH}_2)\text{C}_5\text{H}_4\text{N})_2\text{Cu}_2(\mu_2\text{-OOCMe}_3)_4$ (**2**, C_6H_6) and $((3\text{-NH}_2)\text{C}_5\text{H}_4\text{N})_2\text{Cu}_2(\mu_2\text{-OOCMe}_3)_4$ (**3**) and the cocrystallization product $((4\text{-NMe}_2)\text{C}_5\text{H}_4\text{N})_2\text{Cu}(\eta^2\text{-OOCMe}_3)_2 \cdot 2((4\text{-NMe}_2)\text{C}_5\text{H}_4\text{N})_2\text{Cu}_2(\mu_2\text{-OOCMe}_3)_4$ (**4**) were synthesized by the reaction of the polymer $[\text{Cu}(\text{OOCMe}_3)_2]_n$ (**1**) with aminopyridine ligands (L) of different nature (Cu: L = 1:1) in C_6H_6 . The solid-state thermal decomposition of these compounds was studied by differential scanning calorimetry and thermogravimetry, and their electrochemical behavior was investigated by cyclic voltammetry. All newly synthesized complexes were studied by X-ray diffraction, the magnetic properties of the complexes were investigated, and ESR measurements were performed.

© 2010 Elsevier Ltd. All rights reserved.

1. Introduction

In recent years, the use of metal complexes as molecular precursors for the preparation of nanosized metal particles [1,2] has attracted great interest because of the unique physical and catalytic properties [3–5] of such metallic materials. The solid-phase thermolysis of solutions of complex molecular precursors in suitable matrices [6–10] is used for the synthesis of metals as often as the gas-phase decomposition [1,11] or, for example, the sol–gel technologies [2]. However, the solid-state thermal decomposition of complexes containing metal cations in the absence of external reducing agents differs in that the organic components of precursors play an important role in this process. For instance, it is known that metals can easily be generated in the final step of thermal decomposition using complexes with ligands having strong reducing properties. This approach has recently been applied to the thermolysis of methylhydrazine 3d-metal complexes, which afforded metals or even alloys (in the case of the co-thermolysis of the complexes) [12] at rather low temperatures (below 400 °C). Presumably, these reactions proceed *via* the intramolecular reduction of metals with the involvement of ligands having reducing properties.

* Corresponding author. Tel.: +7 (495) 955 4835; fax: +7 (495) 952 1279.

E-mail address: fomina@igic.ras.ru (I. Fomina).

¹ Fax: +7 (383) 333 1399.

² Tel.: +7 (495) 939 3065; fax: +7 (495) 932 8846.

A rise of the temperature leads to a gradual elimination of organic fragments and the clustering of the metal core up to the formation of metal particles. Evidently, these processes essentially depend on the nature of metal ions in the precursors, as well as on the structural and electronic features of both the ligands having a reducing ability and the molecules as a whole.

As for the known type of carboxylate complexes, *viz.*, dinuclear tetrabridged d-block metal pivalates $\text{LM}(\mu\text{-Piv})_4\text{ML}$, where $\text{M} = \text{Mn(II)}$ [13,14], Fe(II) [15], Co(II) [16–18], Ni(II) [19,20], or Cu(II) [21,22], it can be noted that the pivalate ligand ($\text{Piv} = (\text{CH}_3)_3\text{CCO}_2^-$) is a potential reducing agent with respect to metal ions because it contains a large number of C–H bonds. However, it appeared that the nature of the metal ions, as well as the axial ligand, also play an important role. For example, the solid-phase thermolysis of dinuclear manganese and iron pivalates ($\text{M} = \text{Mn}$ and Fe) did not afford metals in spite of the presence of strong reducing agents (aminopyridine ligands) as the ligands L [23]. On the other hand, the thermolysis of tetrabridged dinuclear complexes with nickel atoms sometimes afforded a metallic phase [24].

In the present study, we focused on the influence of the nature of the ligands L on the phase composition of thermolysis products and investigated the electrochemical behavior of a series of dinuclear copper pivalates $\text{LCu}(\mu\text{-Piv})_4\text{CuL}$ (L is substituted pyridine). The results of this study allow the evaluation of the pathways of the transformations of these molecules in the course of thermal redox processes.

2. Experimental

2.1. Synthesis

The synthetic operations were carried out under pure argon in oxygen-free solvents using the standard Schlenk technique. Starting copper pivalate **1** was synthesized according to a procedure described earlier [21]. The synthesis of new compounds was carried out with the use of trimethylacetic acid (Acros Organics), 2-aminopyridine, 3-aminopyridine, and 4-dimethylaminopyridine (Aldrich).

2.1.1. $((2-NH_2)C_5H_4N)_2Cu_2(\mu-OCCMe_3)_4 \cdot C_6H_6$ (**2**· C_6H_6)

Benzene (40 mL) was added to a mixture of polymer **1** $[Cu(OCCMe_3)_2]_n$ (0.331 g, 1.169 mmol; per formula unit $Cu(OCCMe_3)_2$) and 2-aminopyridine (0.109 g, 1.169 mmol), and the reaction mixture was stirred at 80 °C until the reagents were completely dissolved. The solution was concentrated to 15 mL and kept at room temperature for 24 h. Green crystals suitable for X-ray diffraction were gathered, washed with cold C_6H_6 , and dried under a stream of argon. The solvate of compound **2** with one C_6H_6 molecule was obtained in a yield of 0.477 g (96%). *Anal. Calc.* for $C_{36}H_{54}Cu_2N_4O_8$: C, 54.25; H, 6.82; N, 7.02. *Found*: C, 54.29; H, 6.91; N, 7.09%. IR (KBr) ν/cm^{-1} : 3480 m, 3360 m, 3336 s, 3200 s, 2968 s, 2952 m, 2908 m, 2868 m, 1644 s, 1620 s, 1580 s, 1572 s, 1536 s, 1496 s, 1480 s, 1452 s, 1408 s, 1372 m, 1356 m, 1336 m, 1268 m, 1228 m, 1160 m, 1080 w, 1052 w, 1016 m, 952 w, 936 w, 896 m, 848 m, 804 m, 792 m, 776 s, 744 w, 680 m, 652 m, 620 m, 548 m, 516 m, 456 m, 400 w, 364 w, 356 w, 320 w.

2.1.2. $((3-NH_2)C_5H_4N)_2Cu_2(\mu-OCCMe_3)_4$ (**3**)

Benzene (30 mL) was added to a mixture of polymer **1** $[Cu(OCCMe_3)_2]_n$ (0.3 g, 1.129 mmol; per formula unit $Cu(OCCMe_3)_2$) and 3-aminopyridine (0.105 g, 1.129 mmol), and the reaction mixture was stirred at 80 °C until the reagents were completely dissolved. The solution was concentrated to 15 mL and kept at room temperature for 24 h. Green crystals suitable for X-ray diffraction were gathered, washed with cold C_6H_6 , and dried under a stream of argon. The yield of compound **3** was 0.390 g (96%). *Anal. Calc.* for $C_{30}H_{48}Cu_2N_4O_8$: C, 50.11; H, 6.72; N, 7.78. *Found*: C, 50.16; H, 6.80; N, 7.82%. IR (KBr) ν/cm^{-1} : 3432 m, 3364 m, 3268 m, 2968 s, 2960 s, 2928 m, 2868 m, 1684 s, 1600 s, 1484 s, 1448 s, 1416 s, 1376 m, 1360 m, 1316 m, 1272 m, 1224 m, 1196 m, 1132 w, 1076 w, 1052 w, 1020 m, 936 w, 896 m, 856 m, 796 m, 788 s, 696 m, 644 m, 620 m, 548 m, 520 m, 440 m, 416 w, 392 w, 352 w, 316 w.

2.1.3. Cocrystallization product $[((4-NMe_2)C_5H_4N)_2Cu_2(\mu-OCCMe_3)_4 \cdot 0.5Cu(\eta^2-OCCMe_3)_2((4-NMe_2)C_5H_4N)_2]$ (**4**)

Benzene (40 mL) was added to a mixture of polymer **1** $[Cu(OCCMe_3)_2]_n$ (0.331 g, 1.169 mmol; per formula unit $Cu(OCCMe_3)_2$) and 4-dimethylaminopyridine (0.143 g, 1.169 mmol), and the reaction mixture was stirred at 80 °C until the reagents were completely dissolved. The solution was concentrated to 15 mL and kept at ~5 °C for 24 h. Green crystals were gathered, washed with cold C_6H_6 , and dried under a stream of argon. The yield of compound **4** was 0.493 g (96%). *Anal. Calc.* for $C_{92}H_{150}Cu_5N_{12}O_{20}$: C, 53.59; H, 7.33; N, 8.15. *Found*: C, 53.62; H, 7.36; N, 8.14%. IR (KBr) ν/cm^{-1} : 3482 m, 3364 m, 3332 s, 2968 s, 2980 s, 2956 s, 2924 s, 2868 m, 2816 m, 1684 m, 1620 s, 1604 s, 1572 s, 1540 s, 1536 s, 1444 s, 1416 s, 1392 s, 1372 m, 1364 m, 1360 m, 1340 m, 1228 m, 1160 w, 1116 m, 1068 m, 1008 s, 980 w, 952 m, 936 w, 896 m, 888 m, 804 s, 788 m, 756 m, 680 m, 676 m, 616 m, 544 w, 524 m, 488 w, 432 m, 388 w, 352 w, 312 w.

Crystal suitable for X-ray diffraction was chosen from those precipitated from the benzene mother liquor.

2.2. Methods

Microanalyses were carried out on a Euro Vector Element CHN analyzer (Model EA 3000). The IR spectra were recorded on a Spectord M80 spectrometer in KBr pellets ($4000-300\text{ cm}^{-1}$). Magnetic measurements were performed on a Quantum Design MPMSXL SQUID magnetometer in the 2–300 K temperature range at a magnetic field strength of 5 kOe. The paramagnetic components of the magnetic susceptibility χ were calculated taking into account the diamagnetic contribution estimated from the Pascal constants. The effective magnetic moment was calculated by the equation $\mu_{\text{eff}} = \left(\frac{3k}{N_A\beta^2} \cdot \chi T\right)^{1/2} \approx (8\chi T)^{1/2}$ where N_A , β , and k are Avogadro's number, the Bohr magneton, and the Boltzmann constant, respectively. The Q-band ESR spectra were recorded on a Bruker Elexsys E580 spectrometer (34 GHz) equipped with a standard EN 5107D2 resonator and an Oxford Instruments cryostat for cooling. All experiments were carried out with the use of polycrystalline samples, which were pre-dried with argon to remove the mother liquor (for approximately 1 min) and sealed in quartz tubes *in vacuo*. The calculations were performed using the EasySpin program package [25]. The thermal decomposition of compounds was studied by differential scanning calorimetry (DSC) and thermogravimetric analysis (TGA) on DSC-20 and TG-50 units of a Mettler TA-3000 thermoanalyzer. In all experiments, samples of the compounds were heated under dry argon at a constant rate of 5 deg/min. For each compound, two DSC experiments and three TG experiments were performed. The weight loss upon thermal degradation was determined directly on a TG-50 unit; the accuracy of weighing was $\pm 2 \cdot 10^{-3}$ mg. The thermal decomposition was studied in steps by differential scanning calorimetry, which involved the division of the total temperature range into intervals. The size and number of these intervals were determined based on the overall patterns of weight loss upon decomposition. This approach allowed us to determine the weight loss in each temperature range and compare the results of DSC with the TG data. The results of these methods were in satisfactory agreement, which confirms the reliability of the experimental data. The accuracy of the determination of anomalous points and thermal effects in the DSC curves was $\pm 1^\circ$ and $\pm 0.5\%$, respectively. The X-ray powder diffraction analysis of the decomposition products was carried out on a FR-552 monochromator chamber ($CuK_{\alpha 1}$ radiation) using germanium as the internal standard (X-ray diffraction patterns were processed on an IZA-2 comparator with an accuracy of ± 0.01 mm) and with the use of the STOE Powder Diffraction System. The electrochemical oxidation and reduction potentials were measured with a digital IPC-Win potentiostat/galvanostat connected to a personal computer. The voltammograms were recorded in acetonitrile with 0.05 M *n*-Bu₄NBF₄ as a supporting electrolyte at 20 °C in 8 mL-electrochemical cell. Oxygen was removed from the solutions by purging with dry argon. Working electrode was a stationary platinum disk with a surface area of 0.049 cm². A platinum plate was used as an auxiliary electrode, and a saturated silver chloride electrode was used as the reference electrode (the potential with respect to Fc/Fc⁺ = –0.46 V in CH₃CN). The measured potentials were corrected for ohmic losses. The number of electrons involved in each step of the electrochemical process was determined by the ferrocene reference method.

2.3. X-ray data collection

The X-ray data sets for complexes **2**· C_6H_6 , **3**, and **4** were collected according to a standard procedure [26] on a Bruker AXS SMART 1000 APEX II diffractometer equipped with a CCD detector

(graphite monochromator, ω scanning technique, scan step 0.3°, exposure time per frame 10 s). For all complexes, semiempirical absorption corrections were applied (min/max transmission was 0.7088/0.9181 for **2**·C₆H₆, 0.7374/0.9100 for **3**, and 0.7010/0.9008 for **4**) [27]. The structures of all complexes were solved by direct methods and using Fourier techniques and were refined by the full-matrix least squares against F^2 with anisotropic thermal parameters for all non-hydrogen atoms (except for the carbon atoms of the solvent molecules in structures **2**·C₆H₆ and **4** and the carbon atoms of one disordered *tert*-butyl group (each C atom of the methyl groups in the *tert*-butyl substituent group was located in two positions with occupancy factors of ~0.5)). The hydrogen atoms in complexes **2**·C₆H₆, **3**, and **4** were positioned geometrically and refined using the riding model. In all structures, there is a rotational disorder of the *tert*-butyl groups of the pivalate ligands (formally due to rotation about the single C–CMe₃ bond), which is strongly manifested in the anisotropic temperature factors of the C atoms of the *tert*-butyl groups. In all crystal structures, all bond lengths in the *tert*-butyl groups were constrained to be equal to the bond lengths between the corresponding atoms (the apparent standard deviation was 0.03 Å). The benzene molecules of solvation in the refinement were fitted to a regular hexagon (with $d = 1.39$ Å) in structure **2**·C₆H₆. In addition, there are disordered solvent molecules (apparently, benzene) in structure **4**. The calculations were carried out with the use of the SHELX97 program package [28]. The crystallographic parameters and the X-ray data collection and refinement statistics for the structures of **2**·C₆H₆, **3**, and **4** are given in Table 1.

3. Results and discussion

3.1. Synthesis and X-ray diffraction study

It is known that aminopyridines act as reducing agents [29] and readily undergo condensation with carbonyl-containing organic moieties [29]. Since pivalate complexes containing carbonyl fragments served as the starting compounds for the thermolysis, we introduced aminopyridine ligands with different structures into dinuclear copper pivalates by the reactions of the known polymer [Cu(OOCCMe₃)₂]_n (**1**) [21,22] with 2-amino- (L¹), 3-amino- (L²), and 4-dimethylaminopyridine (L³) in the ratio Cu:L = 1:1 in nonpolar benzene. In the first two cases, the reaction proceeds virtually

quantitatively to give green crystals of dinuclear copper carboxylate complexes with aminopyridines having the composition ((2-NH₂)C₅H₄N)₂Cu₂(μ-OOCCMe₃)₄ (**2**) (the complex was isolated as a solvate with one benzene molecule (2·C₆H₆)) and ((3-NH₂)C₅H₄N)₂Cu₂(μ-OOCCMe₃)₄ (**3**). In spite of the ratio Cu(OOCCMe₃)₂:L³ = 1:1, only crystals of the cocrystallization product Cu(η²-OOCCMe₃)₂((4-NMe₂)C₅H₄N)₂·2((4-NMe₂)C₅H₄N)₂Cu₂(μ-OOCCMe₃)₄ (**4**) consisting of mono- and dinuclear complexes were isolated by crystallization after the reaction of L³ with polymeric copper pivalate **1**.

According to X-ray diffraction data, dinuclear complexes **2** and **3** with the ligands L¹ and L² are structurally similar in spite of the fact that the pyridine rings in these ligands contain the amino group in different positions (Fig. 1, Table 2).

It should be noted that both structures are characterized by the presence of hydrogen bonding between the protons of the amino groups and the oxygen atoms of the carboxylate bridges (intramolecular in **2**, N–H...O(OOCR) 2.929–3.002 Å; the N–H...O angles are 136.2–155.4°; intermolecular in **3**, N–H...O(OOCR) 3.028–3.110 Å; the N–H...O angles are 116.5–128.4).

The crystal of the cocrystallization product Cu(η²-OOCCMe₃)₂((4-NMe₂)C₅H₄N)₂·2((4-NMe₂)C₅H₄N)₂Cu₂(μ-OOCCMe₃)₄ (**4**) (Fig. 2, Table 2) consists of two different complex molecules, viz., the dinuclear molecule ((4-NMe₂)C₅H₄N)₂Cu₂(μ-OOCCMe₃)₄ (**4a**) located on a crystallographic center of symmetry and the mononuclear molecule Cu(η²-OOCCMe₃)₂((4-NMe₂)C₅H₄N)₂ (**4b**) having the crystallographic symmetry C_{2h}. Although the overall structure of the dinuclear molecule (**4a**) differs only slightly from the structures of dinuclear complexes **2** and **3**, the distance between the copper atoms in molecule **4a** (Cu...Cu, 2.664(3) Å) is somewhat longer than those in complexes **2** and **3** (Cu...Cu, 2.6307(9) and 2.6360(18) Å, respectively). It is noteworthy that the Cu–N distance between the copper atom and the nitrogen atoms of the pyridine ligands in the dinuclear molecule (**4a**) (2.138(10) Å; N–Cu...Cu, 179.3(3)°) is essentially different from the Cu–N distance in mononuclear complex **4b** containing the *trans*-coordinated pyridine ligands (Cu–N, 2.00(2) Å), whereas this distance is approximately equal to the corresponding distances in **2** and **3** (2.163(5), 2.177(5) Å and 2.155(10), 2.161(10) Å, respectively).

As opposed to complexes **2** and **3**, the hydrogen bonding in compound **4** is absent.

All newly synthesized copper complexes **2–4** contain strong donor aminopyridine ligands in the coordination sphere. However, it

Table 1
Crystallographic data and details of the structure refinement for complexes **2**·C₆H₆, **3** and **4**.

Complex/parameter	2 ·C ₆ H ₆	3	4
Formula	C ₃₆ H ₅₄ Cu ₂ N ₄ O ₈	C ₃₀ H ₄₈ Cu ₂ N ₄ O ₈	C ₉₂ H ₁₅₀ Cu ₅ N ₁₂ O ₂₀
Formula weight	797.91	719.80	2061.94
T (K)	200(2)	296(2)	296(2)
Crystal system	monoclinic	monoclinic	monoclinic
Space group	Cc	P2(1)/n	C2/m
a (Å)	35.539(2)	9.6551(10)	20.4591(14)
b (Å)	11.7266(6)	20.554(2)	30.797(2)
c (Å)	29.472(1)	18.9913(19)	10.9921(8)
β (°)	100.020(1)	101.977(2)	114.8860(10)
V (Å ³)	12095.4(11)	3686.9(7)	6282.8(8)
Z	12	4	2
D _{calc} (g cm ⁻³)	1.315	1.297	1.090
μ (mm ⁻¹)	1.087	1.201	0.889
Total number of reflections/unique	35 134/23 135	24 315/7598	22 373/6647
R _{int}	0.0427	0.0984	0.1626
θ _{max} (°)	26.73	26.73	26.73
S	0.996	0.969	1.000
R ₁ [I > 2σ(I)]	0.0673	0.0618	0.0832
wR ₂ [I > 2σ(I)]	0.1675	0.1014	0.1569
R ₁ (all data)	0.0915	0.1302	0.1411
wR ₂ (all data)	0.1872	0.1792	0.1749

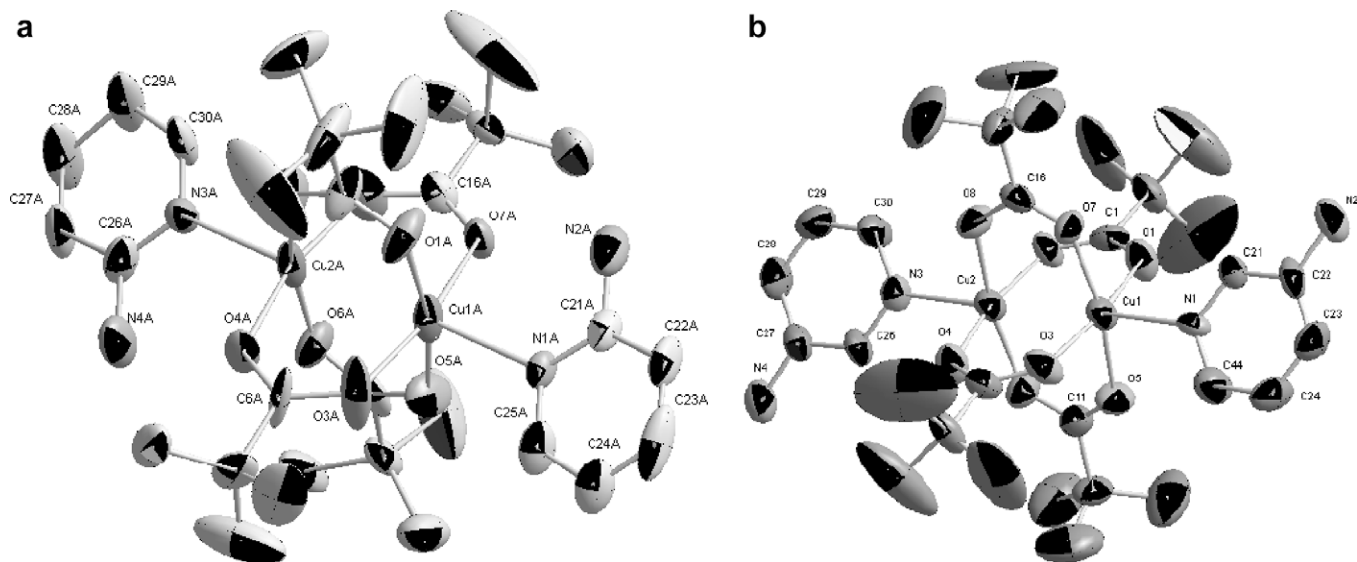


Fig. 1. Structures of the dinuclear complexes $((2\text{-NH}_2)\text{C}_5\text{H}_4\text{N})_2\text{Cu}_2(\mu\text{-OOCCMe}_3)_4$ (**2**) (a) and $((3\text{-NH}_2)\text{C}_5\text{H}_4\text{N})_2\text{Cu}_2(\mu\text{-OOCCMe}_3)_4$ (**3**) (b) (hydrogen atoms are omitted for clarity).

Table 2

Main structural and magnetic characteristics for the dinuclear copper pivalate complexes.

Compound	Cu...Cu (Å)	Cu–N (Å)	Cu–O (Å)	μ_{eff} (μ_B) 300–2 K.	Exchange parameters- $2J^c$ (cm^{-1})
$((2\text{-NH}_2)\text{C}_5\text{H}_4\text{N})_2\text{Cu}_2(\mu\text{-OOCCMe}_3)_4$ (2) ^a	2.6307(9)	2.163(5), 2.177(5)	1.942(5) – 1.990(5)	2.084 – 0.090	214(7)
$((3\text{-NH}_2)\text{C}_5\text{H}_4\text{N})_2\text{Cu}_2(\mu\text{-OOCCMe}_3)_4$ (3)	2.6360(18)	2.155(10), 2.161(10)	1.937(8) – 1.989(8)	1.993 – 0.085	244(5)
$\text{Cu}(\eta^2\text{-OOCCMe}_3)_2((4\text{-NMe}_2)\text{C}_5\text{H}_4\text{N})_2$ ^b		2.00(2)	1.965(16)	2.519 – 1.254	
$((4\text{-NMe}_2)\text{C}_5\text{H}_4\text{N})_2\text{Cu}_2(\mu\text{-OOCCMe}_3)_4$ ^b	2.664(3)	2.138(10)	1.961(10) – 1.999(9)		214(5)
$(\text{C}_9\text{H}_7\text{N})_2\text{Cu}_2(\mu\text{-OOCCMe}_3)_4$ (5)	2.6543(9) [24]	2.223(3)	1.956(3) – 1.985(2)	1.889 – 0.105 [24]	264(7)
$(2,3\text{-Me}_2\text{C}_5\text{H}_3\text{N})_2\text{Cu}_2(\text{OOCCMe}_3)_4$ (6) [24]				1.883 – 0.088 [24]	261(1)
$((2\text{-NH}_2)(6\text{-CH}_3)\text{C}_5\text{H}_3\text{N})_2\text{Cu}_2(\text{OOCCMe}_3)_4$ (7)	2.730(1) [23]	2.296(3)	1.963(2) – 1.974(2)	1.976 – 0.232	249(0)
$((\text{NH}_2)_2\text{C}_5\text{H}_3\text{N})_2\text{Cu}_2(\text{OOCCMe}_3)_4\cdot\text{C}_6\text{H}_6$ (8)	2.762(1) [23]	2.243(3)	1.922(6) – 2.019(5)	1.920 – 0.171 [23]	256(3)

^a Three independent molecules in unit cell.

^b In the co-crystallizate **4**.

^c Exchange-coupled dimmers model [35].

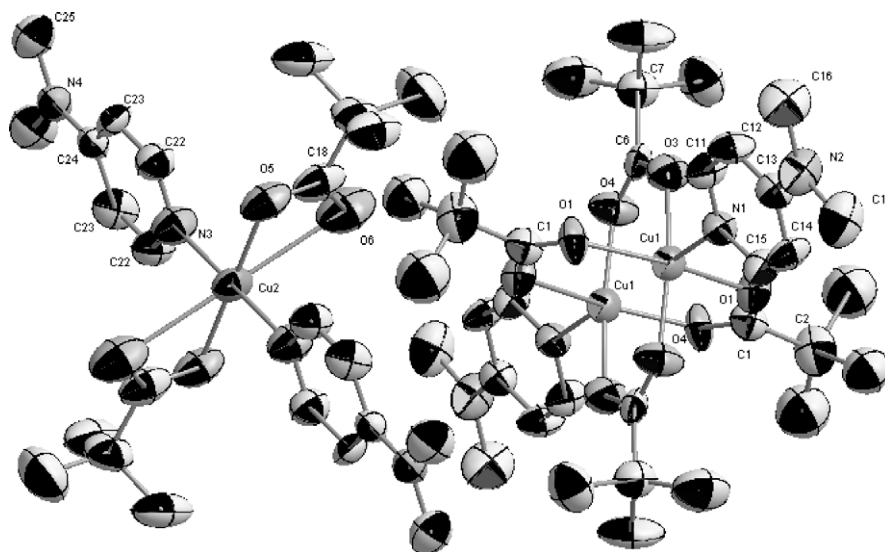


Fig. 2. Structures of the di- and mononuclear molecules (**4a** and **4b**) in the cocrystallization product $\text{Cu}(\eta^2\text{-OOCCMe}_3)_2((4\text{-NMe}_2)\text{C}_5\text{H}_4\text{N})_2 \cdot 2((4\text{-NMe}_2)\text{C}_5\text{H}_4\text{N})_2\text{Cu}_2(\mu\text{-OOCCMe}_3)_4$ (**4**) (hydrogen atoms are omitted for clarity).

should be noted that there are hydrogen bond networks between the protons of the amino groups and the oxygen atoms of the

carboxylate ligands in the crystal structures of dinuclear molecules **2** and **3**, whereas the co-crystallizate consist of discrete dinuclear

and mononuclear complexes and not form hydrogen bonds between the carboxylate and dimethylaminopyridine ligands. In further investigations of the magnetic properties, ESR measurements, and electro- and thermochemical studies, we used not only the above-mentioned complexes but also other dinuclear copper pivalates LCu(Piv)₄CuL (L are pyridine derivatives: quinoline (C₉H₇N) (**5**), 2,3-dimethylpyridine (2,3-(CH₃)₂C₅H₃N) (**6**), 2-amino-6-methylpyridine (2-NH₂)(6-CH₃)C₅H₃N) (**7**), and 2,6-diaminopyridine 2,6-(NH₂)₂C₅H₃N) (**8**)) and the cocrystallization product Cu₂(-Piv)₄(2,6-(NH₂)₂C₅H₃N)₂·Cu₂(Piv)₄(CH₃CN)₂ (**9**), whose synthesis and structures have been described in our recent publications [23,24].

3.2. Magnetic properties

The magnetic properties of dinuclear complexes **2** and **3** differ only slightly from those of the related dinuclear pivalate-bridged copper complexes studied earlier [23,24,30–34,16]. In dinuclear complexes **2**, **3**, and **5–8**, the exchange spin-spin interactions are antiferromagnetic, as clearly seen from the temperature dependences of μ_{eff} (Fig. 3). A lowering of the temperature leads to a decrease in value μ_{eff} ($\mu_{\text{eff}} = 2.084 \mu_{\text{B}}$ (300 K) – 0.090 μ_{B} (2 K) for **2**; $\mu_{\text{eff}} = 1.994 \mu_{\text{B}}$ (300 K) – 0.085 μ_{B} (2 K) for **3**; $\mu_{\text{eff}} = 1.889 \mu_{\text{B}}$ (300 K) – 0.105 μ_{B} (5 K) for **5** [24]; $\mu_{\text{eff}} = 1.883 \mu_{\text{B}}$ (300 K) – 0.088 μ_{B} (5 K) for **6** [24]; $\mu_{\text{eff}} = 1.976 \mu_{\text{B}}$ (300 K) – 0.232

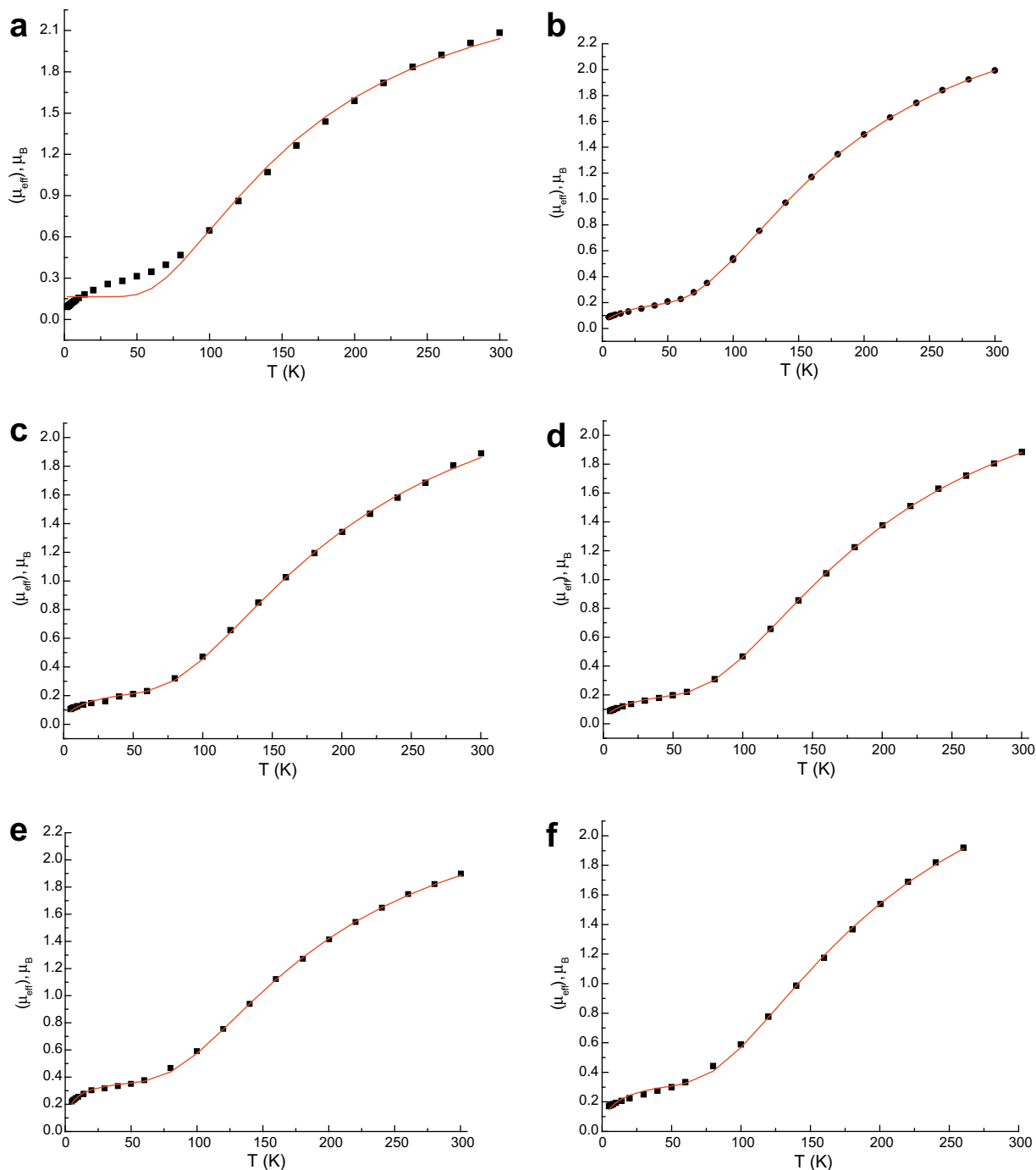


Fig. 3. Temperature dependences of the effective magnetic moment for the complexes ((2-NH₂)C₅H₄N)₂Cu₂(μ-OOCCMe₃)₄ (**2**) (a), ((3-NH₂)C₅H₄N)₂Cu₂(μ-OOCCMe₃)₄ (**3**) (b), (C₉H₇N)₂Cu₂(μ-OOCCMe₃)₄ (**5**) (c), (2,3-Me₂C₅H₃N)₂Cu₂(OOCCMe₃)₄ (**6**) (d), ((2-NH₂)(6-CH₃)C₅H₃N)₂Cu₂(OOCCMe₃)₄ (**7**) (e), and ((NH₂)₂C₅H₃N)₂Cu₂(OOCCMe₃)₄·C₆H₆ (**8**) (f), (● are experimental values, — is the theoretical curve).

μ_B (5 K) for **7**; $\mu_{\text{eff}} = 1.920 \mu_B$ (260 K) – $0.171 \mu_B$ (5 K) for **8** [23]; and $\mu_{\text{eff}} = 2.693 \mu_B$ (300 K) – $0.120 \mu_B$ (2 K) for **9** [23]). The parameters of exchange interactions were estimated using a model of exchange-coupled dimers [35]. The values of exchange parameters obtained are given in Table 2.

Compound **4** was obtained as a result of cocrystallization of the dinuclear and mononuclear complexes in a ratio of 2:1 {(Cu–Cu) + 1/2 Cu}. For cocrystallization product **4**, the temperature dependence of μ_{eff} is shown in Fig. 4. At 300 K, the value of μ_{eff} is $2.52 \mu_B$. A lowering of the temperature leads to a decrease in the value of μ_{eff} , which reaches the value $1.35 \mu_B$ at 70 K, after which μ_{eff} remains virtually unchanged down to helium temperatures (at 5 K, the value of μ_{eff} is $1.25 \mu_B$ (Table 2)).

The paramagnetism of compound **4** is associated with the presence of unpaired electrons of Cu^{II} ions in both dinuclear and mononuclear complexes. As in the case of compounds **2**, **3**, and **5–8** (Fig. 3), the dependence $\mu_{\text{eff}}(T)$ in the 300–70 K temperature range for **4** is determined by antiferromagnetic spin–spin exchange interactions in **4a**, resulting in the spin pairing in **4a** at temperatures below 70 K. The residual μ_{eff} value ($\sim 1.3 \mu_B$) in the 70–5 K temperature range is determined primarily by the unpaired electrons of Cu^{II} in complex **4b**. In the solid-phase of **4**, the intermolecular spin–spin exchange interactions between complexes **4a** and **4b** can be ignored, and the contributions from the dinuclear and mononuclear complexes to χ can be estimated as $\chi(\text{Cu–Cu}) + \chi(\text{Cu})$. The component $\chi(\text{Cu})$ was evaluated from the Curie–Weiss law using temperature dependence of the inverse magnetic susceptibility in the 5–25 K temperature range, where the contribution of the dinuclear complex to the magnetic susceptibility can be ignored. We analyzed the dependence $1/\chi(T)$ (based on the first eight values) and obtained the values $C = 0.20771 \text{ K cm}^3/\text{mol}$ and $\theta = -0.37381 \text{ K}$ (Fig. 4b). The C value is in good agreement with the theoretical value ($0.2057 \text{ K cm}^3/\text{mol}$) determined for one-half mole of the noninteracting paramagnetic centers with the spins $S = 1/2$ and the g factor of 2.10. The parameter of exchange interaction in **4a** was estimated with the use of the model of exchange-coupled dinuclear complexes taking into account the contribution from the mononuclear complex.

The obtained values for parameter of exchange interaction J ($-214(5) \text{ cm}^{-1}$) has the same order of magnitude as the corresponding parameters for complexes **2**, **3**, and **5–8** (Table 2).

For cocrystallization product **9**, the average parameter of exchange interaction was estimated, both exchange clusters being assumed to be equal. The obtained values for parameter of exchange interaction J is $-268(4) \text{ cm}^{-1}$.

3.3. ESR spectra

The electron spin resonance (ESR) is widely used to study magnetic interactions in exchange-coupled paramagnetic clusters [36]. Generally, the information obtained by ESR refers to the determination of g -tensors parameters and dipole interaction parameters (zero-field splitting tensor D); however, in some cases, the exchange interactions and their signs were determined as well [37,38]. The information on symmetry of the environment of paramagnetic ions and the contribution of the anisotropic exchange interactions can be obtained by analyzing the components of the g and D tensors. Hence, we performed systematic studies and a comparative analysis of a series of dinuclear tetrabridged copper pivalate complexes **2–7** and **9** by Q-band ESR spectroscopy (34 GHz).

The ESR spectra of compounds **2–7** and **9** are typical of the state with the total electron spin $S = 1$ and a large zero-field splitting. The intensity of the observed signals of the triplet ($S = 1$) state, which are unambiguously assigned to the dinuclear copper complexes under study, decreases with decreasing temperature, and these signals are difficult to observe at temperatures below ≈ 70 – 100 K . This fact is in complete agreement with the results of magnetic susceptibility measurements and is indicative of the singlet ground state of the copper dimers (unobservable by ESR) and the antiferromagnetic exchange. Hence, all compounds were studied at room temperature (293 K) and at $T = 150 \text{ K}$. The low-temperature experiments, in which the spectral lines are substantially narrower, allowed us to more precisely determine the magnetic resonance parameters of the systems. However, the ESR spectra are very difficult to record at $T < 150 \text{ K}$ due to depletion of the excited triplet state. In addition, the experiments performed at two temperatures showed that the parameters of the copper dimers in the complexes under study depend only slightly on the temperature.

Fig. 5 shows the experimental and theoretically approximated ESR spectra of complexes **2–7** and **9** at $T = 293$ and 150 K . All spectra are essentially similar, except for the spectrum of cocrystallization product **4**, which shows not only the signal of the triplet state ($S = 1$) but also the typical signal of the magnetically isolated copper ion. The very similar ESR spectra of the complex $[\text{Cu}(\text{Sup})_2\text{H}_2\text{O}]_2$ were interpreted earlier [39]. Let us mention the following main features: (1) the intense signals in a field $B_0 \approx 950$ and 1350 mT correspond to the allowed transitions with $\Delta M = 1$, and the splitting between these lines is caused by the electron dipole–dipole interaction (zero-field splitting); (2) the signals in a field $B_0 \approx 500 \text{ mT}$ correspond to the forbidden

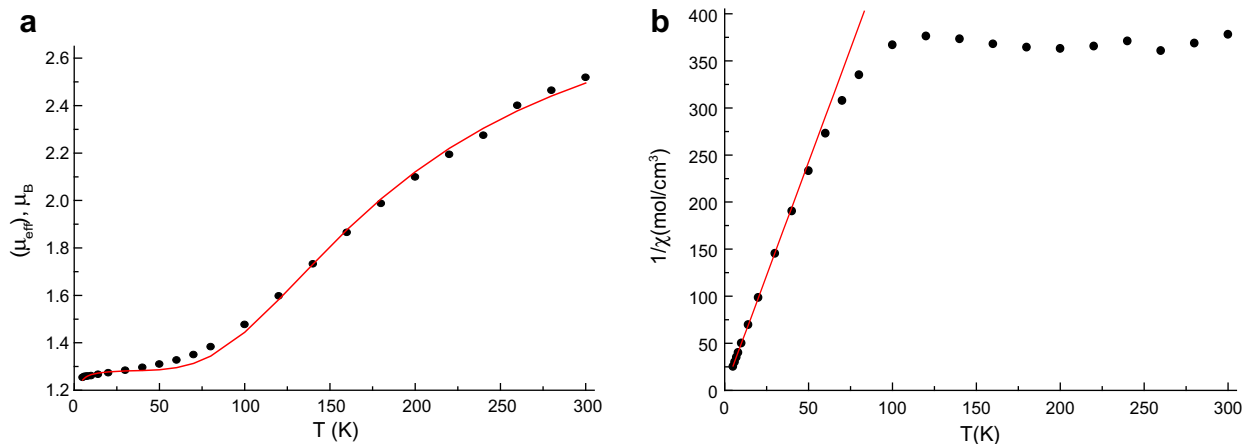


Fig. 4. Temperature dependences of μ_{eff} (a) and the inverse magnetic susceptibility $1/\chi$ (b) for compound **4** (● are experimental values, — is the theoretical curve).

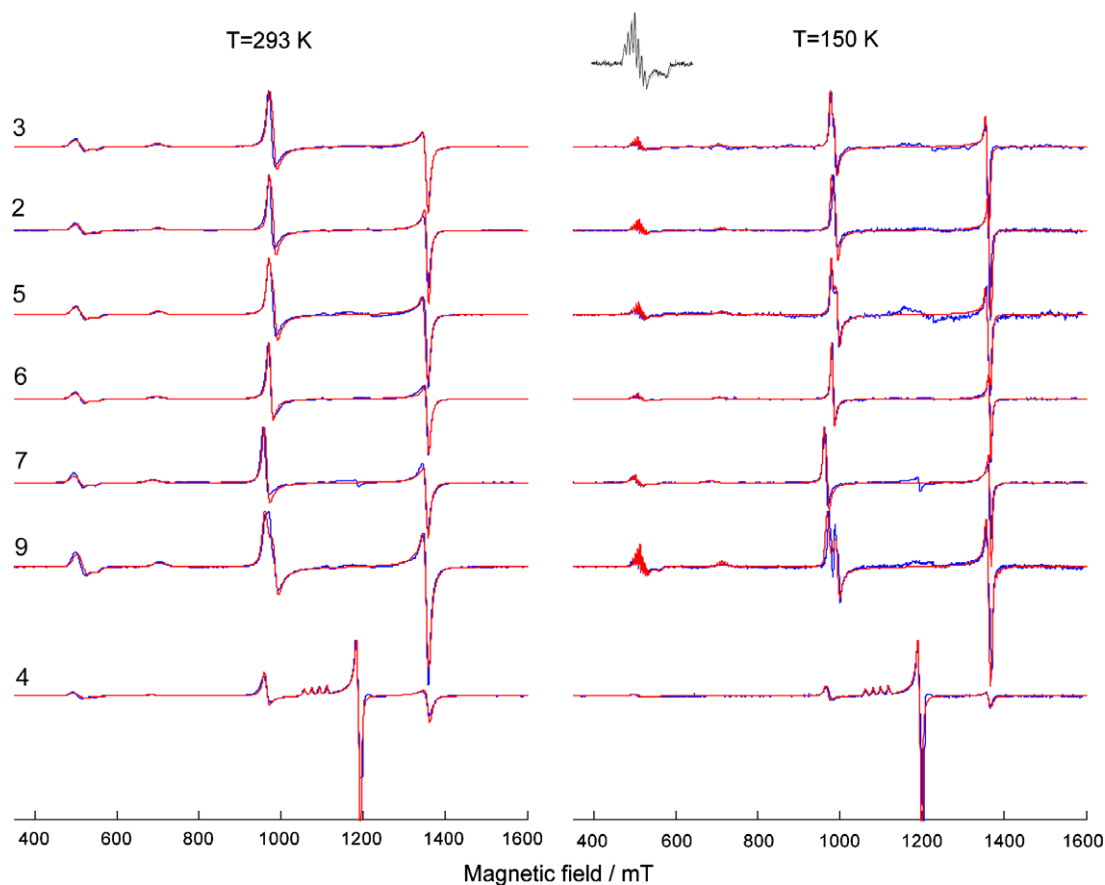


Fig. 5. Experimental (—) and calculated (---) ESR spectra of compounds **2–7** and **9** at 293 K (on the left side, $\nu_{\text{mw}} \approx 34.2$ GHz) and 150 K (on the right side, $\nu_{\text{mw}} \approx 34.4$ GHz).

double-quantum transitions with $\Delta M = 2$ typical of triplet states; (3) the low-intensity signals in a field $B_0 \approx 1100$ – 1200 mT (**2**, **3**, **5–7**, and **9**) also correspond to double-quantum transitions; however, the contribution of insignificant impurities of free copper ions, which can give signals at the same magnetic field strength, cannot be ruled out.

In the calculations, the model took into account the total electron spin $S = 1$, which is coupled with two equivalent ^{63}Cu nuclei with the corresponding hyperfine coupling tensors and has a zero-field splitting commonly described by the scalar parameters D and E . All tensors were assumed to be collinear, which was sufficient for obtaining good agreement with the experimental data, and the g tensor was assumed to be nearly axially symmetrical. However, in some cases, it was necessary to take into account the rhombic distortion to reach agreement with experimental data and, consequently, to take into account the non-zero parameter E .

As a rule, in copper ions, the hyperfine coupling constants for the z component of g tensor (A_{zz}) are substantially larger than the constants for the x,y components ($A_{xx,yy}$). As a result, only the A_{zz} values were reliably determined in the calculations from the well-resolved structure of the signals with $\Delta M = 2$ at $T = 150$ K. In all cases, the spectral lines have a Lorentzian line shape, which is indicative of a relaxation broadening.

The calculated magnetic resonance parameters of complexes **2–7** and **9** are given in Table 3. As can be seen from this table, the differences between compounds **2–7** and **9** are, on the whole, small. This result was expected because the magnetic interactions are located in the dinuclear fragment, and the influence of substituents more distant than those involved in the direct coordination environment of the copper ion should not have a substantial effect. This is also confirmed by very similar magnetic susceptibility curves. However, as it follows from the ESR spectra and the components

Table 3
Calculation parameters for the EPR spectra^a of the compounds **2–7**, **9**.

Compound	g -Tensor	D (cm^{-1})	E (cm^{-1})	A_{zz} (MHz)
2	[2.0702.0622.375]	0.387	−0.003	210
3	[2.078 2.062 2.390]	0.385	−0.002	205
4	[2.075 2.075 2.390]	0.404	0	200
	[2.055 2.055 2.253] ^b			580 ^b
5	[2.070 2.062 2.380]	0.383	−0.004	210
6	[2.071 2.067 2.380]	0.391	−0.001	210
7	[2.074 2.066 2.385]	0.408	−0.002	202
9	[2.080 2.060 2.355]	0.390	−0.006	205

^a The accuracy of the parameters determination is estimated to be: ± 0.003 for the g -tensor components, ± 0.002 cm^{-1} for D and E , ± 2 MHz for A_{zz} . The signs of the D and E parameters should be understood as the relative ones, i.e. $[\pm D \pm E]$.

^b Parameters of the magnetically isolated copper(II) ion in the compound **4**.

of the *g* and *D* tensors, the degree of rhombic distortion (i.e., the deviation of the coordination environment of the copper ions from the axial symmetry) slightly varies from compound to compound.

3.4. Cyclic voltammetric studies

Apparently, the solid-state thermal decomposition of molecular precursors, for example, transition metal complexes, including dinuclear metal pivalates, is the redox process, which, in some cases, can lead to reduction of metal ions (up to the metallic phase) and oxidation of organic ligands [22–24,40–42]. The mechanism of these transformations is very complex and is determined primarily by the electronic nature of the precursor components providing the possibility of electron density redistribution in the molecules upon thermal decomposition. Although, the structural parameters of the molecules and the crystal lattice structure often play an important role as well.

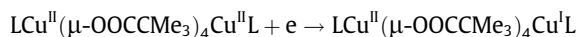
It is reasonable to suggest that the electrochemical reduction and oxidation potentials of precursor complexes are among possible diagnostic criteria for the evaluation of the impact of intramolecular redox processes. Hence, we performed the voltammetric study of the redox behavior (solutions in MeCN) of the dinuclear complexes $\text{LCu}(\mu\text{-Piv})_4\text{CuL}$ (**2–9**), where L is the substituted pyridine.

The potentials of the observed oxidation and reduction peak potentials of the complexes are given in Table 4. The reduction of complexes **1–9** proceeds in two successive one-electron steps, whereas both one- and two-electron waves are observed during oxidation. The oxidation and reduction of complexes **1–9** are irreversible processes, as evidenced by the absence of pronounced peaks in the reverse scans of CV- curves. Consequently, the values presented in Table 4 are not thermodynamic redox potentials. This makes it somewhat difficult to interpret their relation to possible structural rearrangements of the molecules of complexes in solution. However, for a series of compounds containing the structurally and compositionally similar metal carboxylate core $\text{Cu}(\text{Piv})_4\text{Cu}$, certain tendencies in the electron density redistribution in the molecules can be revealed. All peaks present in the voltammograms correspond to the diffusion-limited processes.

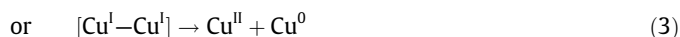
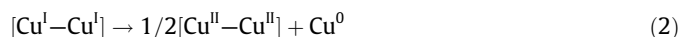
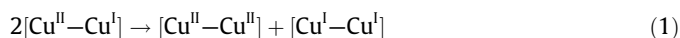
3.4.1. Reduction

The reduction peaks observed in CVs are diffusion-controlled (as follows from $I_p \sim v^{1/2}$ linear dependence (v = scan rate) and, according to the estimation of peak current values, correspond to consecutive one-electron processes. A comparative analysis of the reduction potentials (E_{red}) of the dinuclear copper complexes suggests that, in the case of complexes **1–9**, the reduction of the

copper center is the first step giving rise to an unstable mixed-valence complex.



The formation of the mixed-valence complexes $[\text{Cu}^{\text{II}}\text{Cu}^{\text{I}}]$ has been observed earlier in the reduction of dinuclear Cu(II) tetraacetate complexes [43,45]. The peak potential values for dinuclear complexes **1–9** (Table 4) are shifted in the cathodic direction, thus reflecting the stronger electron-donating properties of the pivalate ligands compared to the acetate ligands but the shapes of CV curves for complexes with pivalate and acetate [43] bridging ligands are similar. A broadening of the reduction peak and the absence of the reoxidation peak in the reverse scan of the cyclic voltammogram indicate that the electron transfer is followed by the structural reorganization of the mixed-valence complex. The structural reorganization can involve both a change in the type of the coordination polyhedron of the copper ions and, for example, the elimination of one of the bridging pivalate ligands. In addition, the complexes $[\text{Cu}^{\text{II}}\text{Cu}^{\text{I}}]$ are prone to disproportionation to form metallic Cu [39,43–45]. However, a weak oxidation peak at a potential of 0.1 V (corresponding to oxidation of Cu^0) was observed for dinuclear complexes **1–9** only at a slow potential scan rate (≤ 50 mV/s), if the scan was reversed after the first reduction peak. This indicates that process (1)



is slow on the CV time scale. However, if the potential scan is reversed after the second reduction peak (corresponding to the formation of the complex $[\text{Cu}^{\text{I}}\text{Cu}^{\text{I}}]$), a very intense oxidation peak of Cu^0 can be observed in the reverse scan (Fig. 6). This is evidence that the disproportionation according to Eq. (2) or (3) goes virtually to completion during the cyclic voltammetry experiments.

It should be noted that the reduction peaks in the voltammograms of complexes **2–9** at -1.2 – -1.5 V potential range assigned to the second electron transfer are strongly broadened, and these peaks are shifted in the cathodic direction by 100–200 mV after repeated scanning. This makes it difficult to precisely determine the redox potential values and is indicative of the occurrence of chemical and adsorption processes accompanying the electron transfer. In this context, Table 4 gives the potential values only of the first reduction peaks observed in the voltammograms.

Since the electron density back-donation from the copper centers to the axial ligand is unlikely to occur in these systems, the ligand acts only as an electron-pair donor. Hence, the reduction

Table 4
Redox properties of compounds **1–9** ($C = 7 \cdot 10^{-4}$ M, CH_3CN , Pt, 100 mV/s, Bu_4NBF_4 , vs. $\text{Ag}/\text{AgCl}/\text{KCl}$).

Complex	$-E_{\text{red}}^{\text{red}}$ (V)	E^{ox} (V)	Decomposition product
Cu_2piv_4 (1) [21,22]	0.68	1.27 1.80	Cu, Cu_2O , CuO
$\text{Cu}_2\text{piv}_4(2\text{-(NH}_2\text{)C}_5\text{H}_4\text{N})_2$ (2)	0.65	1.42	Cu
$\text{Cu}_2\text{piv}_4(3\text{-(NH}_2\text{)C}_5\text{H}_4\text{N})_2$ (3)	0.69	1.39	Cu
Co-crystallization product $\text{Cu}(\eta^2\text{-OOCMe}_3)_2((4\text{-NMe}_2\text{)C}_5\text{H}_4\text{N})_2 \cdot 2((4\text{-NMe}_2\text{)C}_5\text{H}_4\text{N})_2\text{Cu}_2(\mu\text{-OOCMe}_3)_4$ (4)	0.74	1.32	Cu
$\text{Cu}_2\text{piv}_4(\text{C}_9\text{H}_7\text{N})_2$ (5) [24]	0.35	1.39	CuO
$\text{Cu}_2(\text{piv})_4(2,3\text{-Me}_2\text{C}_5\text{H}_3\text{N})_2$ (6) [24]	0.42	1.13 1.51	CuO , Cu_2O , Cu
$\text{Cu}_2(\text{piv})_4((2\text{-NH}_2)(6\text{-CH}_3)\text{C}_5\text{H}_3\text{N})_2$ (7) [23]	0.77	0.97 1.64	Cu
$\text{Cu}_2(\text{piv})_4(2,6\text{-(NH}_2)_2\text{C}_5\text{H}_3\text{N})_2$ (8) [23]	0.95	0.85 1.31	Cu
Co-crystallization product $\text{Cu}_2(\text{piv})_4(2,6\text{-(NH}_2)_2\text{C}_5\text{H}_3\text{N})_2 \cdot \text{Cu}_2(\text{piv})_4(\text{CH}_3\text{CN})_2$ (9) [23]	0.89	0.91 1.31	Cu, Cu_2O

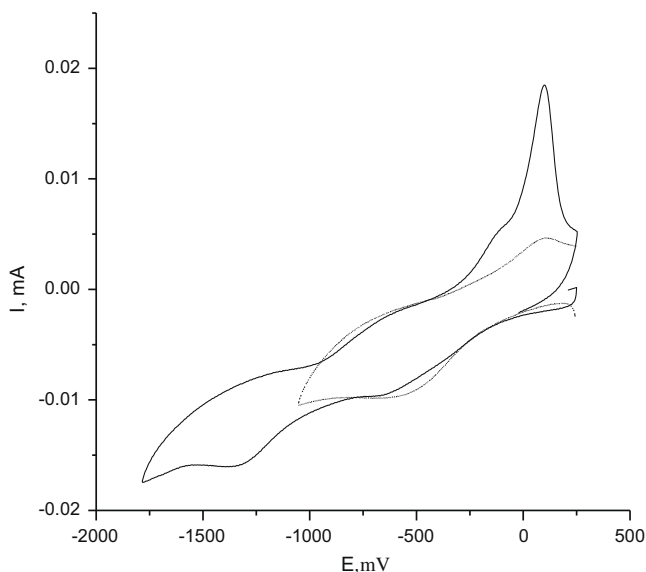


Fig. 6. Typical CV curve for complex **3** (7×10^{-4} M, CH₃CN, 50 mV/s, Pt ($s = 0.049$ cm²), Bu₄NBF₄, vs. Ag/AgCl/KCl).

potential of dinuclear complexes should be shifted to negative values with increasing donating ability of the ligand, which is actually observed in cyclic voltammetry experiments (Table 4). Based on the observed sequence in the reduction potential values of the complexes, it can be concluded that thermal decomposition of more electron-rich complexes (which are reduced at more cathodic potentials) affords products of higher degrees of reduction of Cu(II) ions in pivalate complexes **2–9**. It should be noted that in our case the evaluation of the electron-donating properties of the ligands by analyzing the reduction potentials of the complexes is more correct than a comparison of the oxidation or reduction potentials of the free ligands. This is associated with the fact that pyridine is not oxidized in the potential range under study, and the oxidation of various aminopyridines occurs at the amino group in a rather narrow potential range (0.8–0.9 V, with respect to Ag/AgCl/KCl). According to the literature data [46], the oxidation of amines involves a wide range of consecutive chemical reactions and it impedes the direct comparison of the measured potentials. The reduction of pyridine derivatives containing electron-donating substituents in the ring (which are considered in the present study) occurs at high cathodic potentials (>2.4 V), which also makes it difficult to perform a comparative analysis.

It is worth mentioning that in some cases [38,44] for binuclear copper complexes with carboxylate bridging ligands two sequential two-electron reductions were observed. Such behavior is often the case when binuclear motif is destroyed in solution yielding mononuclear species or if there is no interaction between metallic centers. As follows from the estimation of magnetic properties of complexes **2–9** (see above), it is not our case. Besides, UV–Vis investigation of freshly prepared solutions of the complexes showed that they are stable at least on the timescale of CV measurements.

3.4.2. Oxidation

Although the mechanism of reduction of dinuclear complexes **2–9** seems to be more or less evident, the mechanism of oxidation remains unclear. First, it is worthy of note that both the copper centers and the amino groups of the axial ligands can be oxidized (Scheme 1). The irreversibility of all oxidation peaks indicates that the initially formed electron transfer product is subjected to subsequent fast chemical reactions. As can be seen from Table 4, the

oxidation potentials of the dinuclear copper complexes increase with decreasing donating ability of the axial ligands. Model pivalate polymer **1**, which is transformed into the dinuclear complex (MeCN)Cu(Piv)₄Cu(MeCN) in MeCN solution, is oxidized in one two-electron wave. The structure of the dinuclear complex has been established earlier in cocrystallization product **9** [23]. Since redox-active axial substituents are formally absent in compound **1**, both copper centers apparently undergo oxidation.

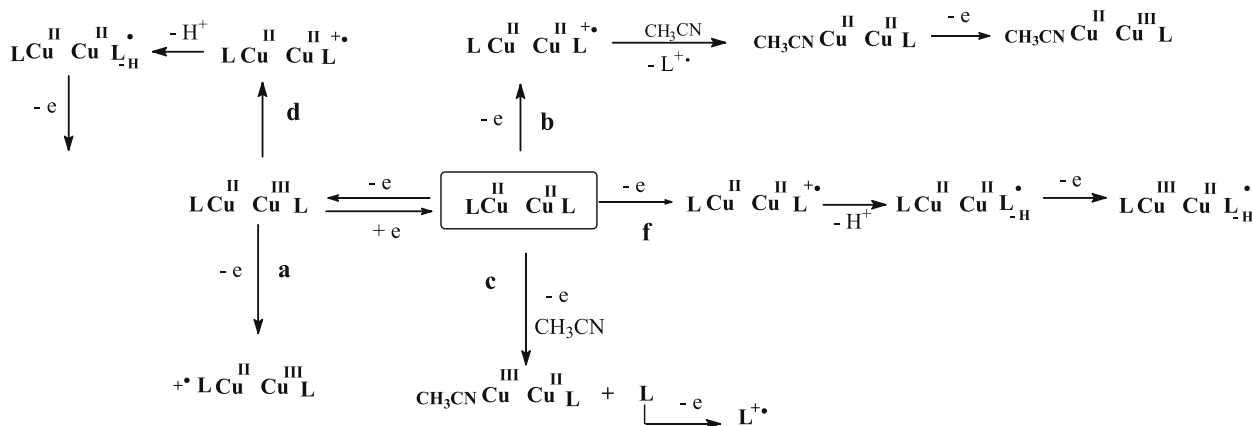
Scheme 1 shows five main possible pathways of oxidation and subsequent fragmentation of dinuclear copper pivalate complexes **2–9**. For simplicity, all ligands containing amino groups in the complexes are designated as L and the pivalate bridges are omitted. In the case of the path **a**, a reversible one-electron oxidation peak corresponding to oxidation of the copper center (because the structure of the complex remains unchanged) followed by oxidation of the axial ligand should be observed in the voltammogram. The path **b** involves the irreversible one-electron oxidation of the ligand followed by its elimination and the replacement by molecules of the solvent (CH₃CN), which is present in a large excess. In the second step, the copper center is oxidized. If the process proceeds according to the mechanism **c**, the first oxidation peak should be two-electron because the ligand that is eliminated (amino-substituted pyridine) is redox-unstable at this potential and, consequently, it should immediately give an electron to the electrode (ECE process: electrochemical step-chemical step-electrochemical step). This means that the oxidized axial ligand is actually eliminated. The driving force for the replacement of the ligand is that the metal in higher oxidation states (metal becomes a harder Lewis acid) is preferably coordinated by the harder base CH₃CN, which is present in a large excess.

The mechanism **f** should involve the irreversible one-electron oxidation of the ligand giving rise to the radical-cation followed by the fast α -proton abstraction (typical of amino- and methyl-substituted pyridines). In the second step, the further one-electron oxidation of the metal center or the ligand can occur.

The path **d** is, in essence, similar to the above-considered path **f**. In the first step, the copper center is oxidized to form a mixed-valence complex followed by the fast intramolecular electron transfer from the axial ligand to Cu(III) to give the ligand radical-cation. The latter rapidly releases the proton, hydrogen-bonded to the oxygen atom of the pivalate bridge. This process can be the driving force for the intramolecular electron transfer. In the second step, the newly formed Cu(II) center in the complex containing the oxidized axial ligand undergoes one-electron oxidation.

Owing to complexity of the observed electrochemical behavior, it is difficult to decide with certainty only from the CV data which of the above-considered mechanisms is true for each of complexes **2–9**. Potential-controlled electrolysis with the identification of products will be more helpful. However, some hypotheses can be proposed. Since one of the aims of the present study was to elucidate the mechanism of intramolecular redox processes occurring during thermal decomposition of pivalate complexes, the mechanisms **d** and **f** (Scheme 1), which involve the intramolecular electron transfer and the α -proton abstraction from the axial ligand, are of the most interest.

Let us compare the oxidation of complexes **5** and **6** containing the apical ligands, which are not oxidized at potentials lower than 2 V (Table 4). For these complexes, the metal orbitals (Cu(II)/Cu(III)) should be involved in the oxidation. As opposed to complex **5**, the cyclic voltammogram of complex **6** shows two one-electron peaks at $E = 1.13$ and 1.51 V. It can be speculated that the methyl substituents of complex **6** play a key role in the difference in the electrochemical behavior of complexes **5** and **6**. Apparently, in the case of complex **6**, Cu(II) is initially oxidized to Cu(III), resulting in an even more substantial donation of electron density from the axial ligand. This, in turn, leads to an increase in the acidity of the



Scheme 1. Possible oxidative transformations of dinuclear copper pivalates.

protons of the methyl group at the α position and a strengthening of the interaction between the oxygen atom of the pivalate bridge and the proton of the methyl group *via* hydrogen bonding. This promotes the intramolecular oxidation of the ligand by the copper center to form the ligand radical-cation accompanied by the fast proton transfer from the ligand to the oxygen atom of the pivalate ligand. The newly formed Cu(II) center again undergoes one-electron oxidation at $E = 1.51$ V. The replacement of the axial ligand by the solvent molecules does not apparently take place because the oxidation potential of the complex is not equal to the oxidation potential of model pivalate complex **1**, which does not contain heterocyclic apical ligands.

The oxidation of complex **3** proceeds in one two-electron step. This suggests that the oxidation of complex **3** follows the path **c**. For compounds **2**, **4**, **7**, **8**, and **9** containing the easily oxidizable axial aminopyridine ligands, it is difficult to draw a definite conclusion. Both the mechanisms **d** and **c** are possible. The fact that the thermal decomposition of these compounds affords metallic copper agrees well with both the strong electron-donating ability of the ligands (see the reduction potentials of the complexes in Table 4) and the presence of α -H atoms that facilitate the intramolecular electron transfer from the ligand to the metal (see above).

Therefore, the electrochemical study of the properties of complexes **1–9** led to the following conclusions. First, a comparative analysis of the first reduction peak potential values of the complexes shows that they reflect the electron-donating properties of the axial ligands and allow the prediction of the impact of intramolecular redox processes during the thermal decomposition of this type of compounds. Second, the analysis of the possible mechanisms of electrochemical oxidation of complexes **1–9** shows that the presence of highly acidic α -H atoms in the axial ligand can facilitate the intramolecular electron transfer from the ligand to the metal, thus increasing the degree of reduction of Cu ions (up to Cu⁰).

3.5. Thermal decomposition

As follows from the results of the electrochemical study, copper pivalate complexes with strong donor axial aminopyridine ligands **2–4** can serve as promising molecular precursors for the preparation of metallic copper by the thermolysis of these complexes *via* intramolecular redox transformations. However, in the first step we performed thermal decomposition of the starting pivalate coordination polymer **1**, which consists of the dinuclear complex units Cu(Piv)₄Cu linked to each other by intermolecular Cu–O_{piv} bonds [22] and which contain no additional ligands with reducing properties, as the model compound.

The thermogravimetric analysis showed that the solid-state decomposition of compound **1** under argon does not afford stable intermediates (Fig. 7a), proceeds in a rather narrow temperature range (230–300 °C), and is endothermic (Fig. 7b). In the 300–365 °C temperature range, highly exothermic processes occur, which may be associated with the formation of new structures of solid decomposition product. The weight loss upon thermolysis is $73.3 \pm 1.5\%$. The phase composition of the final solid decomposition product determined by X-ray powder diffraction shows the presence of a mixture of metallic copper and copper oxides: Cu, Cu₂O, and CuO. Although it is impossible to precisely determine the ratio of the phases in the decomposition products, the thermogravimetric analysis showed that the weight of the solid product after heating of **1** under an inert atmosphere is $26.7 \pm 2.0\%$ of the initial weighed sample, which is equal, within experimental error, to the value of 27.20% calculated from the empirical formula on the assumption that the decomposition affords a mixture of the phases Cu, Cu₂O, and CuO in a ratio of 1:1:1.

Our results differ from the results of the earlier study, in which the thermolysis of polymeric copper pivalate was investigated under a stream of nitrogen by the simultaneous TGA–DTGA–DSC

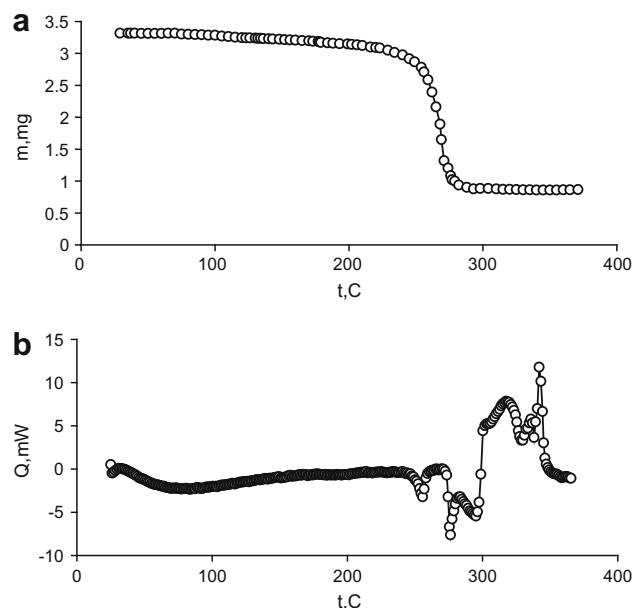


Fig. 7. Temperature dependences of the weight loss (a) and the heat flow (b) for the polymer [Cu₂(Piv)₄]_n (**1**).

(thermogravimetric analysis – differential thermogravimetric analysis – differential scanning calorimetry) method on a Q-1500 D instrument; the heating rate was 2.5 deg/min (the final temperature of the investigation was not reported). Under the above-described thermolysis conditions, metallic copper was not detected, and the final mixture consisted only of oxides Cu_2O and CuO [47].

The present study showed that even the thermolysis of polymeric copper(II) pivalate (**1**) is accompanied by intramolecular redox processes. It can be expected that the presence of pyridine ligands containing easily oxidizable amino groups, which can act as inner-sphere reducing agents, in the dinuclear system $\text{Cu}(\text{Piv})_4$ would lead to deeper intramolecular redox transformations during the thermal decomposition.

It appeared that complexes **2** and **3** containing aminopyridine ligands decomposed in the same manner. It is practically impossible to isolate individual decomposition steps (Fig. 8). It should be noted that an endothermic effect is observed in the curves of heat flow (37–90 °C) (Fig. 8c). The endothermic effect in this temperature range is not associated with decomposition of the samples, as evidenced by a comparison of the TGA (thermogravimetric analysis) curves and DSC (differential scanning calorimetry) curves. Apparently, this effect is attributed to the breaking of hydrogen bonds that are present in the crystals of **2** and **3**. The decomposition of the complexes started at temperatures above 170 °C (**2**) and 208 °C (**3**) (Fig. 8), the onset of decomposition being accompanied by melting (the first endothermic effect (Fig. 8b)). The further deep decomposition proceeds in a rather broad temperature range (170–350 °C and 208–350 °C for **2** and **3**, respectively) and is loss in this temperature range is $80.7 \pm 2.0\%$ and $81.2 \pm 2.0\%$ for **2** and **3**, respectively. The phase composition of the final solid decomposition product determined by X-ray powder diffraction shows that metallic copper was obtained as the only decomposition product. The thermogravimetric analysis showed that the weight of the solid product after heating in an inert atmosphere is $19.3 \pm 2.0\%$ and $18.8 \pm 2.0\%$ of the initial weighed sample, which is equal, within experimental error, to the value of 17.66% calculated from the empirical formula on the assumption that the decomposition afforded metallic copper.

The decomposition of cocrystallization product **4** (Fig. 9) upon heating starts at temperatures above 186 °C, the onset of decomposition being accompanied by melting. As in the case of compounds

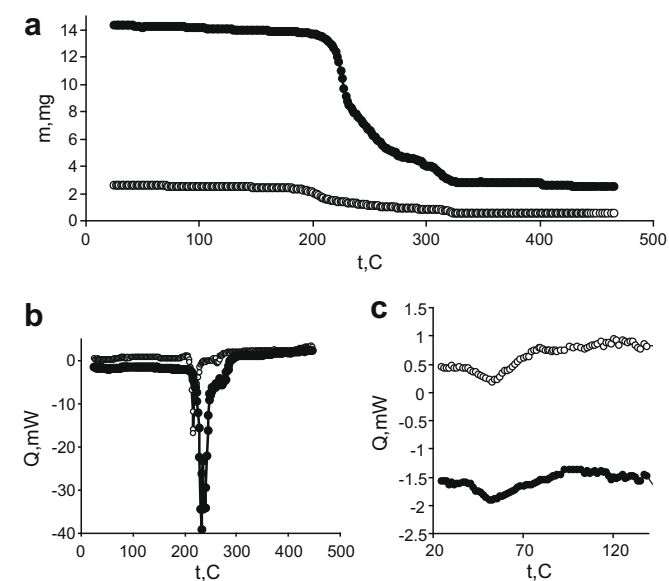


Fig. 8. Temperature dependences of the weight loss (a) and the heat flow (b) for the copper complexes (○ – **2**, ● – **3**).

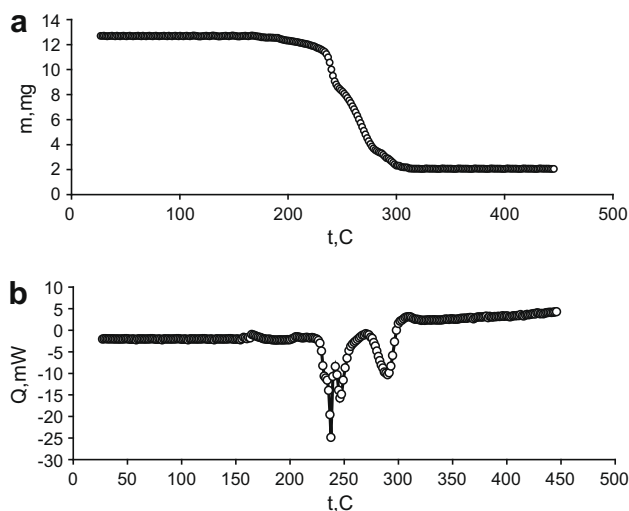


Fig. 9. Temperature dependences of the weight loss (a) and the heat flow (b) for copper complex **4**.

2 and **3**, it is practically impossible to isolate individual decomposition steps. The deep decomposition proceeds in a rather broad temperature range (210–350 °C) and is accompanied by the appearance of a complex endothermic effect (Fig. 9b). The weight loss in this temperature range is $85.1 \pm 1.5\%$. The phase composition of the final solid decomposition product determined by X-ray powder diffraction shows that metallic copper was obtained as the only decomposition product.

Therefore, the study of the thermolysis of complexes **1–4** showed that the introduction of aminopyridine ligands containing easily oxidizable substituents into the coordination sphere of the metal atoms leads to a higher degree of intramolecular redox processes.

An analysis of the results of the present study showed that the temperature of the onset of decomposition of complexes **2–9** is lower than the boiling point of the free ligand (substituted pyridine), the decomposition of all complexes, except for **6**, being accompanied by melting (Table 5). The thermal stability of complexes **2–9** depends on the position and nature of the substituents in pyridine (Table 5). The complexes can be classified into two groups according to this feature. The complexes belonging to the first group (**2**, **3**, **5**, and **6**) contains substituents at positions 2 and 3 (*ortho* and *meta*). There is a correlation between the boiling point of the ligand in these complexes and the temperature of the onset of decomposition of the complexes (Fig. 10). The decrease in the temperature of the onset of decomposition of the complexes belonging to this group [$\Delta = (T_{\text{b.p. of ligand}} - T_{\text{onset of decomposition}})$] is 37.2 °C for **2**, 40 °C for **3**; 31 °C for **5**, and 10.7 °C for **6**.

The second group of complexes (**7–9**) is characterized by the presence of substituents at positions 2 or 6 (*ortho* or *ortho'*). The presence of two substituents in the *ortho* and *ortho'* positions leads to a substantial decrease in the temperature of the onset of decomposition of the complexes [$\Delta = (T_{\text{b.p. of ligand}} - T_{\text{onset of decomposition}})$] (80 °C for **7**, 146 °C for **8**, 145 °C for $((\text{NH}_2)_2\text{C}_5\text{H}_3\text{N}_2)$, and 34 °C (CH_3CN) for **9**).

It was shown that the phase composition of the solid decomposition products of complexes **2–9** is determined by the nature of the substituents in pyridine [23,24]. As demonstrated previously, only copper oxide is generated from complex **5** upon decomposition. The presence of active alkyl substituents in the apical pyridine molecules in complex **6** substantially influences the character of the thermolysis products. The decomposition of **6** affords a mixture of metallic copper and its oxides. The introduction of aminopyridine ligands into the coordination sphere of copper (in complexes

Table 5
Characteristics of the thermolysis processes for compound 1–9.

Complex	$T_{\text{b.p. of N-ligand}} (^{\circ}\text{C})$	$T_{\text{onset of decomposition}} (^{\circ}\text{C})$	Decomposition product
Cu_2piv_4 (1) [21,22]			Cu, Cu_2O , CuO
$\text{Cu}_2\text{piv}_4(2\text{-(NH}_2\text{)C}_5\text{H}_4\text{N})_2$ (2)	207.2;	170	Cu
$\text{Cu}_2\text{piv}_4(3\text{-(NH}_2\text{)C}_5\text{H}_4\text{N})_2$ (3)	248	208	Cu
Co-crystallization product $\text{Cu}(\eta^2\text{-OOCMe}_3)_2((4\text{-NMe}_2\text{)C}_5\text{H}_4\text{N})_2$ (4)	> 191.2;	186	Cu
$\text{Cu}_2\text{piv}_4(\text{C}_9\text{H}_7\text{N})_2$ (5) [24]	238;	207	CuO
$\text{Cu}_2(\text{piv})_4(2,3\text{-Me}_2\text{C}_5\text{H}_3\text{N})_2$ (6) [24]	163.7;	153	CuO , Cu_2O , Cu
$\text{Cu}_2(\text{piv})_4(2\text{-(NH}_2\text{)(6-CH}_3\text{)C}_5\text{H}_3\text{N})_2$ (7) [23]	208;	128	Cu
$\text{Cu}_2(\text{piv})_4(2,6\text{-(NH}_2\text{)}_2\text{C}_5\text{H}_3\text{N})_2$ (8) [23]	285	139	Cu
Co-crystallization product $\text{Cu}_2(\text{piv})_4(2,6\text{-(NH}_2\text{)}_2\text{C}_5\text{H}_3\text{N})_2 \cdot \text{Cu}_2(\text{piv})_4(\text{CH}_3\text{CN})_2$ (9) [23]	285 81	140 (for $(\text{NH}_2)_2\text{C}_5\text{H}_3\text{N}_2$) 115 (for CH_3CN)	Cu, Cu_2O

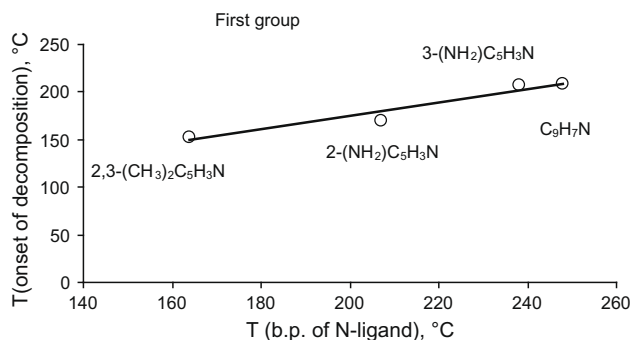


Fig. 10. Plot of the temperature of the onset of decomposition vs. the boiling point of the ligand for complexes **2**, **3**, **5**, and **6**.

2–4, **7**, and **8**) results in a higher degree of intramolecular redox processes and the formation of metallic copper as the only solid decomposition product. The appearance of Cu_2O among the thermolysis products of complex **9** is apparently attributed to the presence of the acetonitrile complex in cocrystallization product **9**. At the same time, the presence of the complex containing the diaminopyridine ligand in the cocrystallization product stimulates the formation of metallic copper and is, apparently, responsible for the absence of copper(II) oxide, which is formed upon thermolysis of Cu(II) pivalates with quinoline **5** and lutidine **6** or upon decomposition of **1**.

To sum up, we showed that dinuclear pivalate copper(II) complexes **2–9** containing pyridine derivatives as the axial ligands decompose upon heating, their thermolysis proceeding as the intramolecular redox process. In some cases, this results in reduction of Cu(II) ions to Cu_2O or metallic copper and oxidation of organic ligands. The voltammetric study of the redox behavior of the dinuclear complexes $\text{LCu}(\mu\text{-OOCMe}_3)_4\text{CuL}$ (**2–9**), where L is substituted pyridine, confirmed the intramolecular redox mechanism of the solid-phase thermolysis.

4. Supplementary data

CCDC 763453, 763454 and 763455 contain the supplementary crystallographic data for compounds **2**, **3**, and **4**. These data can

be obtained free of charge via <http://www.ccdc.cam.ac.uk/conts/retrieving.html>, or from the Cambridge Crystallographic Data Center, 12 Union Road, Cambridge CB2 1EZ, UK; fax: +44 1223 336 033; or e-mail: deposit@ccdc.cam.ac.uk.

Acknowledgments

This study was financially supported by the Russian Foundation for Basic Research (Project No. 07-03-00408, 07-03-00707, 08-03-00365, 08-03-00343, 08-03-00142, and 08-03-00326), the Council on Grants of the President of the Russian Federation (NSH-3672.2010.3) the Target Programs for Basic Research of the Presidium of the Russian Academy of Sciences and the Division of Chemistry and Materials Science of the Russian Academy of Sciences, Federal agency for science and innovation (State Contract 02.513.12.3098).

References

- [1] C. Brèchignac, P. Houdy, M. Lahmani, *Nanomaterials and Nanotechnology*, EMRS, 424, Springer-Verlag, Berlin Heidelberg, 2007.
- [2] C.B. Murray, C.R. Kagan, M.G. Bawendi, *Annu. Rev. Mater. Sci.* 30 (2000) 545.
- [3] N. Herron, D.L. Thorn, *Adv. Mater.* 10 (1998) 1173.
- [4] C. Desvauz, C. Amiens, P. Fejes, P. Renaud, M. Respaud, P. Lecante, E. Snoeck, B. Chaudret, *Nat. Mater.* 4 (2005) 750.
- [5] D. Cahen, G. Hodes, *Adv. Mater.* 14 (2002) 789.
- [6] R. Padiyath, J. Seth, S.V. Babu, L.J. Matienzo, *J. Appl. Phys.* 73 (1993) 2326.
- [7] R. Dlecohier, H. Van den Bergh, *Appl. Surf. Sci.* 43 (1989) 61.
- [8] S.A. Gromilov, S.V. Korenev, I.A. Baidina, *Russ. J. Struct. Chem.* 3 (2002) 527.
- [9] S.A. Gromilov, S.V. Korenev, I.V. Korolkov, K.V. Yusenko, I.A. Baidina, *Russ. J. Struct. Chem.* 3 (2004) 508.
- [10] B.P. Tolochko, A.Yu. Gaponov, B.B. Bohonov, V.P. Isupov, K.A. Tarasov, M.R. Sharaphutdinov, S.S. Shatskaya, *J. Surf. Invest. X-ray Synchrotron and Neutron Tech.* 3 (2001) 20.
- [11] O.Yu. Gorbbenko, S.I. Troyanov, A. Meets, A.A. Bosak, *Polyhedron* 16 (1997) 1999.
- [12] B. Takayuki, O. Yutaka, T. Yasutaka, *Mater. Chem. Phys.* 78 (2003) 645.
- [13] M.A. Kiskin, I.G. Fomina, G.G. Aleksandrov, A.A. Sidorov, V.M. Novotortsev, Yu.V. Rakitin, Zh.V. Dobrokhotova, V.N. Ikorskii, Yu.G. Shvedenkov, I.L. Eremenko, I.I. Moiseev, *Inorg. Chem. Commun.* 8 (2004) 89.
- [14] I.L. Eremenko, M.A. Kiskin, I.G. Fomina, A.A. Sidorov, G.G. Aleksandrov, V.N. Ikorskii, Yu.G. Shvedenkov, Yu.V. Rakitin, V.M. Novotortsev, *J. Cluster Sci.* 16 (2005) 331.
- [15] A.A. Sidorov, I.G. Fomina, G.G. Aleksandrov, Yu.V. Rakitin, V.M. Novotortsev, V.N. Ikorskii, M.A. Kiskin, I.L. Eremenko, *Russ. Chem. Bull.* 53 (2004) 483.
- [16] Y. Cui, D.L. Long, X.Y. Huang, F.K. Zheng, W.D. Chen, J.S. Huang, *Chinese J. Struct. Chem.* 18 (1999) 107.
- [17] E.V. Pakhmutova, A.E. Malkov, T.B. Mikhailova, A.A. Sidorov, I.G. Fomina, G.G. Aleksandrov, V.M. Novotortsev, V.N. Ikorskii, M.A. Kiskin, I.L. Eremenko, *Russ. Chem. Bull.* 52 (2003) 2105.
- [18] I.G. Fomina, G.G. Aleksandrov, Zh.V. Dobrokhotova, O.Yu. Proshenkina, M.A. Kiskin, Yu.A. Velikodny, V.N. Ikorskii, V.M. Novotortsev, I.L. Eremenko, *Russ. Chem. Bull.* 55 (2006) 1909.
- [19] I.L. Eremenko, S.E. Nefedov, A.A. Sidorov, I.I. Moiseev, *Russ. Chem. Bull.* 48 (1999) 405.
- [20] N.I. Kirilova, Yu.T. Struchkov, M.A. Porai-Koshits, A.A. Pasynskii, A.S. Antsyshkina, L.Kh. Minacheva, G.G. Sadikov, T.Ch. Idrisov, V.T. Kalinnikov, *Inorg. Chim. Acta* 42 (1980) 115.
- [21] T.O. Denisova, E.V. Amelchenkova, I.V. Pruss, Zh.V. Dobrokhotova, O.P. Fialkovskii, S.E. Nefedov, *Russ. J. Inorg. Chem.* 7 (2006) 1020.
- [22] E.G. Ilrina, S.I. Troyanov, K.M. Dunaeva, *Russ. J. Coord. Chem.* 18 (1992) 882.
- [23] I.G. Fomina, Zh.V. Dobrokhotova, G.G. Aleksandrov, M.A. Kiskin, M.A. Bikov, V.N. Ikorskii, V.M. Novotortsev, I.L. Eremenko, *Russ. Chem. Bull.* 56 (2007) 1722.
- [24] I.G. Fomina, Zh.V. Dobrokhotova, M.A. Kiskin, G.G. Aleksandrov, O.Yu. Proshenkina, A.L. Emelina, V.N. Ikorskii, V.M. Novotortsev, I.L. Eremenko, *Russ. Chem. Bull.* 56 (2007) 1712.
- [25] S. Stoll, A. Schweiger, *J. Magn. Reson.* 178 (2006) 42.
- [26] SMART (Control) and SAINT (Integration) Software, Version 5.0, Bruker AXS Inc., Madison, WI, 1997.
- [27] G.M. Sheldrick, SADABS, Program for Scanning and Correction of Area Detector Data, Göttingen University, Göttingen, Germany, 1997.
- [28] G.M. Sheldrick, SHELX-97: Program for the Solution of Crystal Structures, Göttingen, Germany, 1997.
- [29] M.B. Smith, J. March, *March's Advanced Organic Chemistry: Reactions, Mechanisms and Structure*, vol. 6, Wiley, Interscience, JohnWiley & Sons, Inc., Publication, 2007, and references cited therein.
- [30] Y. Kani, M. Tsuchimoto, S. Ohba, H. Matsushima, T. Tokii, *Acta Crystallogr., Sect. C: Crystallogr., Struct. Commun.* 46 (2000) 923.

- [31] I.L. Eremenko, M.A. Golubnichaya, S.E. Nefedov, I.B. Baranovsky, I.A. Olshnitskaya, O.G. Ellert, V.M. Novotortsev, L.T. Eremenko, D.A. Nesterenko, *Russ. J. Inorg. Chem.* 41 (1996) 2029.
- [32] A.A. Pasynskii, T.Ch. Idrisov, K.M. Suvorova, V.T. Kalinnikov, *J. Coord. Chem.* 2 (1976) 1060.
- [33] Yu.V. Rakitin, V.T. Kalinnikov, *Modern Magnetochemistry*, Science, St.Peterburg, 1994, pp. 220.
- [34] Y. Zhang, L. Jianmin, Z. Min, Q. Wang, X. Wu, *Chem. Lett.* (1998) 1051.
- [35] B. Bleaney, K.D. Bowers, *Proc. Roy. Soc. A* 214 (1952) 451.
- [36] A. Bencini, D. Gatteschi, *EPR of Exchange Coupled Systems*, Springer-Verlag, Berlin, Germany, 1990.
- [37] M. Fedin, S. Veber, I. Gromov, K. Maryunina, S. Fokin, G. Romanenko, R. Sagdeev, V. Ovcharenko, E. Bagryanskaya, *Inorg. Chem.* 46 (2007) 11405.
- [38] S.L. Veber, M.V. Fedin, A.I. Potapov, K.Yu. Maryunina, G.V. Romanenko, R.Z. Sagdeev, V.I. Ovcharenko, D. Goldfarb, E.G. Bagryanskaya, *J. Amer. Chem. Soc.* 130 (2008) 2444.
- [39] P. Koegerler, P.A.M. Williams, B.S. Parajon-Costa, E.J. Baran, L. Lezama, T. Rojo, A. Mueller, *Inorg. Chim. Acta* 268 (1998) 239.
- [40] M.A. Kiskin, G.G. Aleksandrov, Z.V. Dobrokhotova, V.M. Novotortsev, Yu.G. Shvedenkov, I.L. Eremenko, *Russ. Chem. Bull.* 5 (2006) 779.
- [41] N. Yu, S.E. Kozitsyna, I.A. Nefedov, Z.V. Yakushev, M.N. Vargaftik, I.I. Moiseev, *Mendeleev Commun.* 5 (2007) 261.
- [42] Z.V. Dobrokhotova, I.G. Fomina, M.A. Kiskin, A.A. Sidorov, V.M. Novotortsev, I.L. Eremenko, *Russ. Chem. Bull.* 1 (2006) 250.
- [43] I. Toledo, M. Arancibia, C. Andrade, I. Crivelli, *Polyhedron* 17 (1998) 173.
- [44] S. Perlepes, E. Libby, W.E. Streib, K. Folting, G. Christou, *Polyhedron* 11 (1992) 923.
- [45] C. Dendrinou-Samara, P.D. Jannakoudakis, D.P. Kessissoglou, G.E. Manoussakis, D. Mentrzafos, A. Terzis, *J. Chem. Soc., Dalton Trans.* (1992) 3259.
- [46] M.M. Baizer, H. Lund (Eds.), *Organic Electrochemistry*, Marcel Dekker Inc., New York and Basel, 1983 (Chapter. 15 and 21.1.3.).
- [47] E.G. Ilrina, N.A. Santalova, K.M. Dunaeva, *Russ. J. Inorg. Chem.* 9 (1991) 2301.